Taylor & Francis
Taylor & Francis Group

ORIGINAL RESEARCH

    OPEN ACCESS   Check for updates

The signaling function of IDO1 incites the malignant progression of mouse B16 melanoma

E Orecchini[a], ML Belladonna[a], MT Pallotta[a], C Volpi[a], L Zizi[a], E Panfili[a], M Gargaro[a], F Fallarino[a], S Rossini[a], C Suvieri[a], A Macchiarulo[b], S Bicciato[c], G Mondanelli[a]*, and C Orabona [iD][a]*

[a]Department of Medicine and Surgery, University of Perugia, Perugia, Italy; [b]Department of Pharmaceutical Sciences, University of Perugia, Perugia, Italy; [c]Department of Life Sciences, University of Modena and Reggio Emilia, Modena, Italy

ABSTRACT

Indoleamine 2,3 dioxygenase 1 (IDO1), a leader tryptophan-degrading enzyme, represents a recognized immune checkpoint molecule. In neoplasia, IDO1 is often highly expressed in dendritic cells infiltrating the tumor and/or in tumor cells themselves, particularly in human melanoma. In dendritic cells, IDO1 does not merely metabolize tryptophan into kynurenine but, after phosphorylation of critical tyrosine residues in the non-catalytic small domain, it triggers a signaling pathway prolonging its immunoregulatory effects by a feed-forward mechanism. We here investigated whether the non-enzymatic function of IDO1 could also play a role in tumor cells by using B16-F10 mouse melanoma cells transfected with either the wild-type *Ido1* gene (*Ido1^{WT}*) or a mutated variant lacking the catalytic, but not signaling activity (*Ido1^{H350A}*). As compared to the *Ido1^{WT}*-transfected counterpart (B16^{WT}), B16-F10 cells expressing *Ido1^{H350A}* (B16^{H350A}) were characterized by an *in vitro* accelerated growth mediated by increased Ras and Erk activities. Faster growth and malignant progression of B16^{H350A} cells, also detectable *in vivo*, were found to be accompanied by a reduction in tumor-infiltrating CD8^+ T cells and an increase in Foxp3^+ regulatory T cells. Our data, therefore, suggest that the IDO1 signaling function can also occur in tumor cells and that alternative therapeutic approach strategies should be undertaken to effectively tackle this important immune checkpoint molecule.

Introduction

Malignant melanoma is the most aggressive and lethal skin cancer[1]. It derives from the uncontrolled proliferation of melanocytes, responsible for the production and secretion of the melanin pigment.[2] Albeit a 4% reduction in mortality over the past few years, the incidence of new cases has highly increased in the last decades.[3] Melanoma prognosis and survival crucially depend on the tumor stage at the moment of the diagnosis. For primary melanoma, the 5-year survival rate is 99%, while for patients with metastatic melanoma, it is only 10%.[4] In melanoma development, proliferation and invasion mechanisms are mainly driven by the MAPK signaling cascade (Ras/Raf/MEK/Erk), while the PI3K-AKT pathway, also involved in proliferation and survival, is most active to promote cellular energy metabolism.[5] In particular, Erk and Ras are key molecules of melanoma progression, the first being hyperactivated by autocrine growth factors, and the second mutated into a gain-of-function oncogene in 90% and 15–30% of melanoma cases, respectively.[6]

A therapeutic strategy for late-stage melanoma, which cannot be successfully treated by surgical removal, is targeting the phosphorylation of proliferation-mediating kinases. However, inhibitors of BRAF and other components of the MAPK pathway have shown limited efficacy, recorded only in a minority of patients.[7] Nevertheless, antibodies blocking the CTLA-4 (ipilimumab), or PD-1 (pembrolizumab/nivolumab) immune checkpoints elicit durable responses with improved survival, but only in a subset of patients.[8–10] To increase the immunotherapeutic efficacy, a double-interference on immunosuppressive mechanisms was tried in the randomized phase III study ECHO-301/KEYNOTE-252 by the combined treatment with pembrolizumab and epacadostat, i.e., a catalytic inhibitor of the tolerogenic enzyme indoleamine-2,3 dioxygenase 1 (IDO1). This heme-containing enzyme converts the essential amino acid tryptophan (Trp) into kynurenine (Kyn) and thus initiates an enzymatic cascade for Trp depletion and the production of tolerogenic catabolites (known as kynurenines) causing T cell apoptosis and Treg accumulation.[11–15] However, despite the encouraging clinical results in the early-phase trial, epacadostat failed in preventing IDO1-dependent melanoma immune escape and did not increase progression-free survival (PFS) and overall survival (OS) obtained by pembrolizumab monotherapy.[16,17]

In addition to catalytic activity, IDO1 has a non-enzymatic moonlight function previously documented in dendritic cells (DCs),[18] but so far never investigated in tumors. In DCs, IDO1 acts as both an enzyme and an immunoregulatory signal-transducing molecule by means of its two immunoreceptor tyrosine-based inhibitory motifs (ITIMs).[19,20] When phosphorylated, they serve as docking sites for different molecular partners, which

are associated with IDO1 to mediate different physiological effects. ITIM1 phosphorylation and binding to the protein tyrosine phosphatases SHP-1 and SHP-2 trigger sustained IDO1 expression in a feedforward immunosuppressive loop; in contrast, ITIM2 phosphorylation and binding to the suppressor of cytokine signaling 3 (SOCS3) accelerate proteasomal degradation of IDO1.[19–22] In tumors, there is still no evidence for the ITIM-mediated non-enzymatic function of IDO1. However, the existence of a dynamical equilibrium between its apo-form (namely, the protein without the prosthetic group), and the holo-enzyme (namely, the protein containing the prosthetic group) has been documented in several cell types. Post-translational regulation of IDO1 activity depending on the intracellular heme availability was earlier described in human monocyte-derived macrophages (hMDM).[23] Moreover, a pioneer work by Nelp et al.[24] elegantly quantified the amount of apo-IDO1 in the human ovarian cancer cell-line SKOV3. Finally, for the first-time Wainwright D. and Collaborators distinguished in mouse glioblastoma microenvironment, a tumor-specific non-enzymatic (apo-)IDO1 from an enzymatic (holo-)IDO1 expressed in non-tumor cells (i.e., immune cells), suggesting for the first time that apo/holo IDO1 balance could be cell-specific.[25–27] Therefore, the apo-form of IDO1 has became an attractive target for new generation inhibitors, aiming at preventing IDO1 catalytic activity by blocking the protein in a conformation not suitable for binding to the heme group.[24] The so-called heme-displacing inhibitors have been already successfully tested in several tumor experimental models and offered an alternative approach to the competitive or noncompetitive inhibition of the catalytic site of IDO1.[28] However, apo-IDO1 is not only a target to prevent Trp catabolism, it also represents a suitable conformation for transducing an intracellular signal, as reported in DCs,[19,29] but never investigated in tumors. It has been recently demonstrated that non-enzymatic IDO1, ectopically expressed by the glioblastoma tumor cell line, suppresses antitumor immunity independently of its enzymatic function,[26] thus suggesting an active role of IDO1 apo-form in tumor progression. However, the exact molecular mechanisms, as well as the involvement of the ITIMs-mediated signaling function in tumor progression, have not been explored yet.

Therefore, the need for effective treatments against advanced malignant melanoma, the awareness that the inhibition of IDO1 catalytic function was not successful in phase III clinical trial, and the knowledge that expression of non-enzymatic IDO1 promotes tolerogenic mechanisms for tumor immune escape prompted us to investigate the non-enzymatic IDO1[H350A] mutated protein in the progression of B16-F10 murine melanoma. For the first time, our data provide a proof of concept that the IDO1 signaling function can affect tumor progression besides its enzymatic activity, suggesting alternative therapeutic approaches to effectively tackle this important immune checkpoint molecule.

Materials and methods

Cell lines, cell culture, and plasmid transfection

B16-F10 murine melanoma cell line, provided by ATCC, and all the stably transfected B16 cell lines were cultured in RPMI-1640 medium supplemented with 10% FBS and maintained in a humidified atmosphere at 37°C in 5% CO_2. Lipofectamine 3000 reagent (Thermo Fisher Scientific) and pEF-BOS–based vectors containing either $Ido1^{H350A}$ or $Ido1^{WT}$, generated as previously described,[19] were used for the transfection according to the manufacturer's instructions. The empty pEF-BOS plasmid was used as mock control. After puromycin selection (2 µg/ml) and multiple rounds of limiting dilution cloning, three different single-cell colonies for each genotype (namely, $Ido1^{H350A}$, $Ido1^{WT}$, and mock) were selected and characterized for IDO1 protein expression, enzymatic activity, and cell proliferation. One of the three clones for each genotype was selected for the functional assays described in the manuscript. Stable cell lines were routinely screened to avoid mycoplasma contamination and maintained in culture for up to 10 passages after thawing.

Kynurenine and tryptophan determinations

The enzymatic activity of IDO1 was measured *in vitro* in terms of the ability to metabolize Trp into Kyn. Kyn and Trp concentrations were detected using a Perkin Elmer, series 200 HPLC instrument (MA, USA) combined with a Kinetex® C18 column (250 × 4.6 mm, 5 µm, 100 A; Phenomenex, USA), maintained at the temperature of 25°C and pressure of 1800 PSI. A mobile phase containing 10 mM NaH_2PO_4 pH 3.0 (99%) and methanol (1%) (Sigma-Aldrich), with a flow rate of 1 ml/min, was used and a UV detector identified Kyn and Trp at 360 nm and 220 nm, respectively. The software TotalChrom v. 6.3.1 was used for evaluating the concentrations of Kyn and Trp in samples by means of a calibration curve. The detection limit of the analysis was 0.05 µM for Kyn and 0.5 µM for Trp.

IDO1 protein degradation analysis

Transfected B16 cells were incubated with the protein synthesis inhibitor cycloheximide 40 µg/ml for the time-course analysis of IDO1 protein degradation. Whole-cell lysates (1 x 10^5 cells/sample) were run on SDS/PAGE and electro-blotted onto 0.2 µm nitrocellulose membranes (Bio-Rad, CA, USA). Membranes were probed with a monoclonal antibody specific for mouse IDO1 (Millipore), in combination with an appropriate horseradish peroxidase-conjugated antibody (Millipore), followed by enhanced chemiluminescence (ECL) (Bio-Rad). Anti-β-tubulin (Sigma-Aldrich) was used as a normalizer. Densitometric analysis of specific signals was performed by ChemiDoc XRS+Imaging System (Bio-Rad), within a linear range of blot exposures, selecting the two lowest exposure times required for detecting signals.

Immunoblot, immunoprecipitation, and Ras pull-down

Transfected B16 cells were lysed on ice in a RIPA buffer (50 mM Tris☐HCl, 150 mM NaCl, 1% Nonidet P☐40, pH 7.4) supplemented with the protease and phosphatase inhibitor cocktail Halt™ (Invitrogen). Protein concentration of the cell lysates was quantified by BCA (Bio-Rad) and 15 µg of total proteins were loaded for immunoblots that involved the use of the specific antibodies: monoclonal anti-IDO1 (Millipore), monoclonal anti-SHP-2 (Santa Cruz Technologies),

monoclonal anti-Erk1/2, and anti-pErk1/2 (Thr202, Tyr204) (Cell Signaling) in combination with the appropriate horse-radish peroxidase☐conjugated antibody (Millipore), followed by enhanced chemiluminescence (ECL, Bio-Rad). A monoclonal anti☐β☐tubulin (Sigma☐Aldrich) was used as a normalizer. For the immunoprecipitation experiments, 200 μg of total proteins were incubated for 2 h at 4°C with pre-bound Dynabeads[TM] protein G magnetic beads (Thermo fisher) and the specific antibodies, namely a rabbit polyclonal anti-pIDO1[19,29] or a mouse monoclonal anti-SHP-2 (Santa Cruz Technologies). The Ras Activation Assay Biochem Kit (Cytoskeleton Inc.) was used for the pull-down of Ras-GTP, according to the manufacturer's instructions. Briefly, 300 μg of total proteins were incubated with 10 μl of Raf-RBD beads at 4°C for 1 h. A monoclonal anti-Ras antibody (Cytoskeleton Inc.) was used for the detection of the total Ras protein in both WCL and in pulled-down Ras-GTP samples. The relative amount of active Ras (Ras-GTP) over the total Ras protein levels was evaluated in stably transfected B16 cell lines. In each experiment, the densitometric analysis of specific signals was performed by ChemiDoc XRS + Imagin System (Bio-Rad), within a linear range of blot exposure, selecting the two lowest exposure times required for detecting signals.

Cell proliferation

Cell proliferation was assessed by MTT assay. Briefly, 5×10^4 cells/well were cultured in a time-course experiment and provided with MTT (Sigma-Aldrich) at the indicated times. After 4 hours at 37°C, 100 μL/well of solubilization buffer (SDS 10% in HCl 0.01 N) were added and incubated overnight at 37°C. The day after, cell proliferation was evaluated by measuring the absorbance at 570 nm (TECAN spectrophotometer, Thermo Fisher Scientific).

Scratch wound healing assay

Stably transfected B16 cells were cultured in a 6-well plate to reach a confluence of approximately 90–100%. A 10-μl sterile pipette tip was used to make a scratch line on the monolayer of confluent cells at the bottom of the culture plate. The wound healings were continuously observed for 48 hours using a Nikon Eclipse 50i microscope with a Nikon DS Fi1 camera (Nikon) and acquiring pictures every 2 h. The area of the wound healing was determined by delimiting and measuring the empty spots at the indicated times with Photoshop CS3 (Adobe Systems Inc.) and Image J (NIH) software, respectively.

Soft agar colony formation assay

A soft agar colony formation assay was used for evaluating the capability of untreated B16 tumor cell lines to grow in an anchorage-independent manner. Firstly, the bottom of a 6-well plate was precoated with a mix (1:1 ratio) of 1% agarose solution and 2X complete RPMI-1640 medium. Then, untreated B16 tumor cells were suspended in 2X complete RPMI-1640 medium and 0.6% agarose solution (1:1 ratio) and plated (1×10^4 cells/well) on the precoated 6-well plate. After 14 days, colonies were imaged using an inverted

microscope (Nikon) at low (20X) and high magnification (60X). The size of colonies was analyzed in 20 randomly selected visual fields in each well and measured using the ImageJ software (NIH). Subsequently, the colonies were stained by MTT (1 mg/ml, overnight at 37°C).

Proteomic analysis and computational analysis

Protein extract from transfected B16 cells was obtained by Lysis buffer (50 mM Tris-HCl, pH 7.4, 200 mM NaCl, 1% Nonidet P☐40, 0.5% Na-deoxycholate) supplemented with the protease and phosphatase inhibitor cocktail Halt[TM] (Invitrogen). For each sample, 30 μg of total protein were analyzed by mass spectrometry at the core facility of Istituto Superiore di Sanità (ISS, Rome, Italy). The unit is equipped with the two mass spectrometers Orbitrap Fusion™ and LTQ XL™ Linear Ion Trap, both from ThermoFisher, with additional Electron Transfer Dissociation (ETD) fragmentation. Principal component analysis (PCA) was performed using the prcomp function of R stats package on log2 protein expression levels. Before PCA, to reduce the effect of noise from non-varying proteins, those proteins with a coefficient of variation smaller than the 95th percentile of the coefficients of variation in the entire dataset were removed. The filter retained 341 proteins that are more variable across samples in any of the 3 subsets (i.e., B16[mock], B16[WT], and B16[H350A]). All proteins with at least one not-null expression signal in at least one sample have been labeled based on their expression in B16[mock], B16[WT], and B16[H350A] samples, respectively. The annotation returned 5148 proteins expressed in all cell types, 11 in B16[mock] only, 17 in B16[mock] and B16[WT], 255 in B16[mock] and B16[H350A], 19 in B16[WT] only, 50 in B16[WT] and B16[H350A], and 85 in B16[H350A]. For the 5198 and 5403 proteins expressed in B16[WT] and B16[H350A] and in B16[mock] and B16[H350A], respectively, fold changes have been quantified as the ratio between the median protein expression levels in B16[H350A] and B16[WT] or B16[mock] samples. Statistical significance of differential expressions (i.e., p-values) in B16[H350A] as compared to B16[WT] or B16[mock] samples has been determined using a t-test on the log2 expression levels of proteins with not-null expression signal in at least two B16[H350A] and B16[WT] (or B16[mock]) samples. P-values have been corrected for multiple comparisons using the Benjamini-Hochberg adjustment method as coded in the *p.adjust* function of the R *stats* package. Global supervised clustering was performed using the function *pheatmap* of R *pheatmap* package with Pearson correlation as distance metric and average agglomeration method on log2 expression levels of 276 proteins with adjusted p-value ≤ 0.05 in both comparisons of B16[H350A] with B16[WT] and B16[mock] samples (supplementary Table S1). Protein expression heatmap has been generated with *pheatmap* after row-wise standardization of the expression values. Functional enrichment analysis has been performed using GSEA and gene sets of the Molecular Signature Database Hallmark collection (http://www.gsea-msigdb.org/ gsea/msigdb/collection_details.jsp#H). The GSEA software (http://software.broadinstitute.org/gsea/index.jsp) was applied in preranked mode to the protein list ranked on log2 fold change. Fold changes have been calculated as the ratio between the median expression levels of the 5198 proteins expressed in

B16^{WT} and B16^{H350A} samples. UniProt protein IDs were converted to human gene symbols using the Human_UniProt_IDs_MSigDB.v7.5.1 annotation file. Gene sets were considered to be significantly enriched at FDR ≤ 0.05 when using weighted enrichment statistics and 1,000 permutations of gene sets. Proteomic raw data are available under the following DOI: 10.6084/m9.figshare.20518329. Fold changes and adjusted p-values of proteins from the comparisons of B16^{H350A} with B16^{WT} and B16^{mock} samples are reported in supplementary Tables S2 and S3, respectively.

Animals and melanoma mouse model

Female wild-type C57BL/6 mice (6-weeks old) were purchased from Charles River Breeding Laboratories Italia. All animals were housed and fed under specific pathogen-free conditions in the animal facility of the University of Perugia. All in vivo studies were in compliance with Italian Animal Welfare Assurance (A-3143-01) and Animal Care and Use Committee guidelines of the University of Perugia. On day 0 of the experiment, stably transfected B16 cells were subcutaneously injected (1 × 10^5 per mouse) into the shaved right flank. Before injection, the cell lines were screened for mycoplasma contamination and maintained in culture for up to 1 week after thawing. On day 7, tumor sizes started to be measured by a caliper every other day and the tumor size was calculated based on an ellipsoid formula. On day 15 of the experiment, tumor bearing mice were sacrificed for the ex vivo analysis. Animals showing signs of distress or bearing a tumor volume higher than 2500 mm^3 were euthanized.

Ex vivo analysis of tumor masses

Tumor masses were excised, photographed, weighed, and analyzed by western blot, HPLC analysis, and flow cytometry. For tumor homogenates, the tumor masses were cut into small pieces and gently disrupted in a minimum volume of ice-cold PBS by using a glass pestle until the homogenate should appear cloudy with minimal solid tissue. The resulting homogenate was filtered, centrifuged and the protein concentration was quantified by BCA (Bio-Rad). For western blotting of the specific proteins and the Ras-GTP pull-down 15 µg and 300 µg of tumor homogenate was used, respectively, following the procedures described above. After deproteinization with perchloric acid 10%, 100 µg of tumor homogenate was analyzed by HPLC for Kyn and Trp measurements, as described above.

For flow cytometry, tumor tissues were dissociated by a gentle-MACS^{TM} Dissociator (Miltenyi Biotec) in HBSS (Thermo fisher) containing Collagenase D and DNase I for 10 min at 37°C. Samples were then filtered through a 100-µm nylon filter (BD Biosciences) in RPMI to generate single-cell suspensions, which were subsequently washed with complete RPMI. The frequencies of IFN-γ-producing CD4$^+$ and CD8$^+$ T cells were determined by extra/intracellular staining, after a pretreatment of the cells with PMA (50 ng/ml; Sigma-Aldrich), ionomycin (0.8 µg/ml, Sigma-Aldrich), and brefeldin A (3 µg/ml; eBioscience) for 4 hours at 37°C. Phenotypic characterization of CD8$^+$ and CD4$^+$ T cell subsets was performed by extracellular staining using the following Abs: Fc block (2.4G2; BD Biosciences), APC-labeled anti-CD3 (145–2C11; Biolegend), BV510-labeled anti-CD4 (RM4-5; BD Horizon), APC-Cy7-labeled anti-CD45.2 (BD Biosciences), BV786-labeled anti-CD44 (IM7; BD Horizon), and PerCP-labeled anti-CD8 (BD Biosciences). Subsequently, for the intracellular staining, cells were treated with the Cytofix/Cytoperm kit (BD Biosciences) and stained with Alexa Flour 488-labeled anti-IFNγ (XMG1.2; eBioscience) and PE-labeled anti-FoxP3 (FJK-16s eBiosciences). Samples were acquired by LSR Fortessa (BD Biosciences, CA, USA) flow cytometer, and analyzed by FlowJo analysis software (Tree Star, OR, USA).

Statistical analysis

For statistical analysis, GraphPad Prism 8.0.1 software for Windows (GraphPad) was used. A p-value ≤ 0.05 was considered statistically significant. Data are expressed as the mean ± S.D. and were analyzed by ANOVA followed by the post hoc Bonferroni's test, when more than two experimental conditions were under comparison, while unpaired Student's t-test was used for the analysis of the data comparing two conditions. Tumor volume growth curves were analyzed by two-way repeated measures ANOVA with a post hoc Bonferroni test at each time point. Survival data were analyzed with the log-rank test with the Sidak correction for multiple comparisons.

Results

Generation of a melanoma cell line expressing non-enzymatic IDO1

Although IDO1 expression and activity have been associated with the progression of many tumor types, including melanoma, limited information about the IDO1-mediated signaling function in tumor cells itself is available.[26] To dissect the non-enzymatic role played by IDO1 in the malignant progression, we generated from B16-F10 cells a mouse melanoma cell line expressing a mutated IDO1 variant lacking the catalytic activity (B16^{H350A}). B16-F10 cells, constitutively not expressing endogenous Ido1,[30] were transfected with either wild-type Ido1 gene (B16^{WT}) or empty vector (B16^{mock}) as controls. Multiple rounds of cloning by limiting dilution were performed to ensure the clonal cell population stably expressing the transgene (Figure 1a). The protein expression, the catalytic activity of IDO1, as well as the cell proliferation rate, were preliminarily assessed in three different single-cell colonies of B16^{WT}, B16^{H350A}, and B16^{mock} (supplementary Figure S1a–c). One of each clones, respectively, expressing Ido1^{WT}, Ido1^{H350A}, and the empty vector (mock), was selected for functional assays and thereafter simply named B16^{WT}, B16^{H350A}, and B16^{mock}. Kyn, the first catabolite of tryptophan degradation and the main marker of IDO1 catalytic activity, was dosed in culture supernatants. As opposed to B16^{WT}, B16^{H350A} cells – expressing an IDO1 mutated in the active site – were unable to secrete Kyn, confirming the loss of IDO1 catalytic activity (Figure 1b). When the IDO1 protein expression was analyzed, it appeared to be significantly higher in B16^{H350A} cells
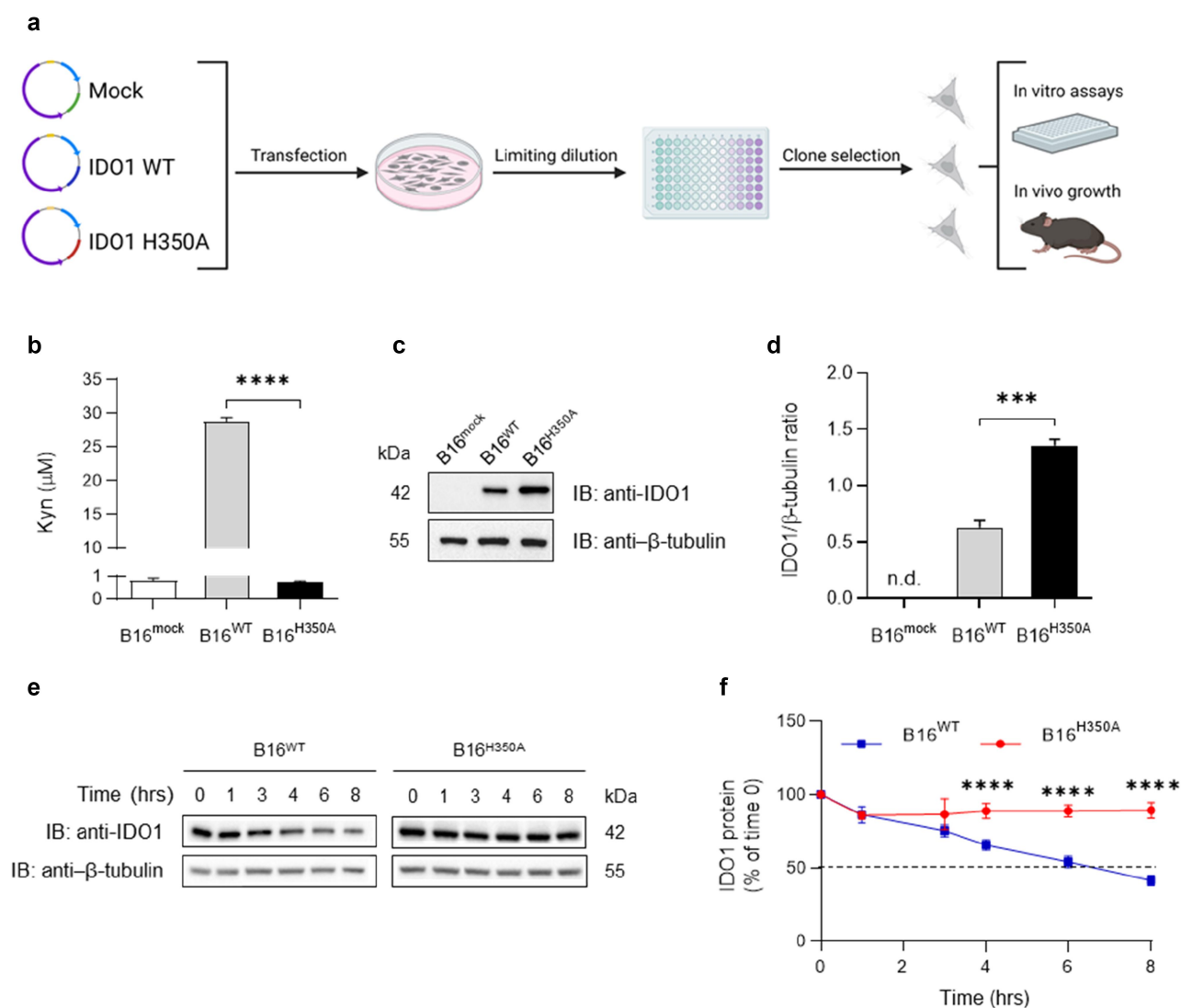
Figure 1. Ectopic expression of non-enzymatic IDO1 in B16 melanoma cell line. (a) Experimental timeline for the generation, selection, and validation of B16-F10 murine melanoma cell clones transfected with either empty vector (B16^{mock}), or wild-type $Ido1$ (B16^{WT}), or mutated $Ido1$ variant lacking the catalytic activity (B16^{H350A}). (b) Production of Kyn is represented as concentration in culture supernatants after incubation for 16 hrs in medium. (c-d) Validation of stably transfected B16^{mock} (white bar), B16^{WT} (gray bar) and B16^{H350A} (black bar) cell lines. For the expression of IDO1 protein, one representative immunoblot of three is shown (c) and IDO1/β-tubulin ratio is graphed (d). (e-f) Reduced half-life of IDO1 in B16^{WT} and B16^{H350A} cells in a cycloheximide-chase assay followed by immunoblot analysis of IDO1 in transfectant lysates. Cycloheximide was added at 40 μg/ml for the indicated time. One representative immunoblot of three is shown (e). (f) Exponential decay regression analysis of the IDO1/β-tubulin ratio for cells treated as in (e) and expressed as percentage of time 0 (time 0 = 100%). Data (mean ± SD) are the results of three independent measurements. Two-tailed unpaired Student's t-test (d), or one-way ANOVA (b), or two-way ANOVA followed by post hoc Bonferroni's test (f) where used for the analysis. *$P < .05$, **$P < .01$. n.d., not detectable.

as compared to the B16^{WT} counterpart, although the same amount of total proteins was loaded (Figure 1c,d). This result suggested that wild-type and non-enzymatic IDO1 might differ in protein stability. Thus, to investigate a possible diverse susceptibility to post-translational degradation, the IDO1 protein decay rate was analyzed by a cycloheximide chase assay followed by immunoblotting. Upon protein synthesis inhibition, the IDO1 protein expression declined more slowly in B16^{H350A} as compared to the B16^{WT} control (Figure 1e). In particular, the non-enzymatic IDO1^{H350A} has a significantly longer half-life ($t_{1/2}$ > 8 h; degradation speed K, 0.009 h^{-1}) than the wild-type protein ($t_{1/2}$ = 6.5 h; degradation speed K, 0.105 h^{-1}) (Figure 1f).

Overall, these results indicated that B16 cells were successfully reconstituted with either a wild-type enzymatically active

or a mutated inactive form of IDO1. The latter was characterized by an altered protein turnover, prolonging both its availability and putative signaling functions in transfected B16-F10 melanoma cells.

Proteomic profiling of melanoma cell line expressing non-enzymatic IDO1

To understand the molecular alterations occurring in the B16^{H350A} cells, the proteomic changes were investigated in the different melanoma cell lines. Therefore, protein samples were extracted from biological quadruplicates of B16^{mock}, B16^{WT}, and B16^{H350A} cell lines and subjected to LC-MS/MS analysis. PCA analysis confirmed the similarity between the replicates and the inter-group differences

(Figure 2a). Moreover, from the analysis of the protein signals, we identified 5148 proteins that are commonly expressed in the three melanoma cell lines, while a total of 85 proteins are exclusively expressed by B16^{H350A} cells (Figure 2b). The heatmap showing statistically significant differences in protein abundances in B16^{H350A}, B16^{WT}, and B16^{mock} cells confirmed a distinct proteomic profile of B16^{H350A} melanoma cells (Figure 2c; supplementary Table S1). We then performed a gene set enrichment analysis (GSEA), searching for statistical associations between the proteins either more or less expressed in the B16^{H350A} as compared to B16^{WT} cells and those contained in a collection of signatures summarizing specific well-defined biological states and processes (see Materials and Methods for details and supplementary Table 2). GSEA analysis suggested that B16^{H350A} compared to B16^{WT}

melanoma cells significantly activate gene sets depicting biological processes linked to cell proliferation and survival. In fact, both gene sets (version 1 and 2) controlled by the oncogene MYC, those modulated by the transcription factor E2F, as well as the G2M checkpoint controlling cell cycle and the DNA repair pathways resulted significantly overrepresented in B16^{H350A} melanoma cells. Differently, the gene sets describing the activation of the immune responses mediated by IFN-γ and IFN-α, the epithelial-mesenchimal transition, and other biological processes such as coagulation, myogenesis, and xenobiotic metabolism resulted significantly under represented (Figure 2d). Overall, the proteomic profile of B16^{H350A} melanoma cells puts in evidence a highly proliferative phenotype in these cells compared to the same tumor cells expressing the wild-type form of IDO1.
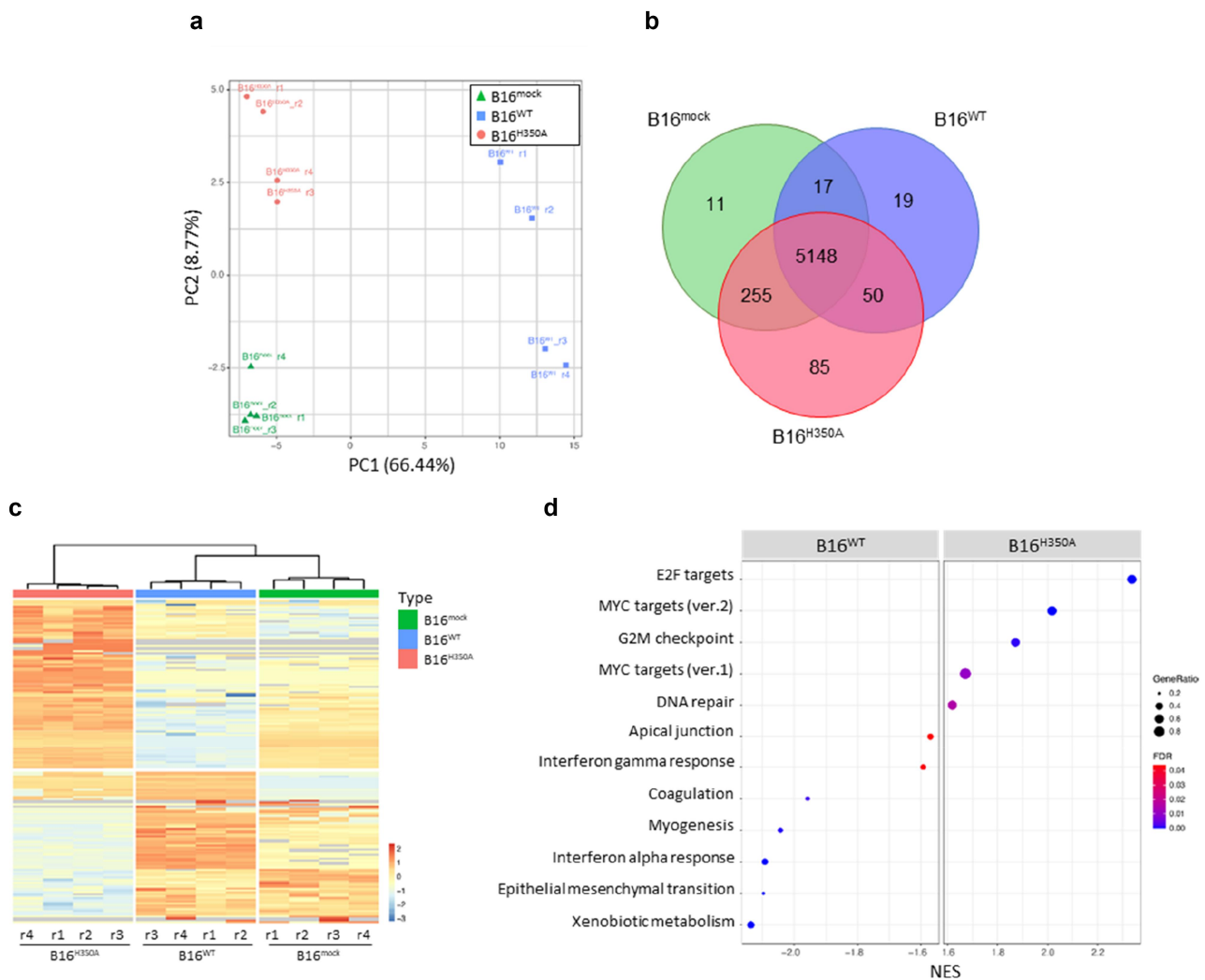

Figure 2. Proteomic profile of B16^{H350A} cells expressing non-enzymatic IDO1. (a) Principal component analysis (PCA) of B16^{H350A}, B16^{mock}, and B16^{WT} protein levels. PCA was performed on log2 protein expression levels. (b) Overlap of proteins expressed in B16^{mock}, B16^{WT}, and B16^{H350A} samples. (c) Supervised hierarchical clustering obtained using the log2 expression levels of 276 proteins with adjusted p-value ≤ 0.05 in both comparisons of B16^{H350A} with B16^{WT} and B16^{mock} samples (supplementary Table S1). Each column represents one separated biological sample. (d) Over-representation analysis was performed using gene set enrichment analysis (GSEA) with the Hallmark signature collection on the ranked protein list of the comparison between B16^{H350A} and B16^{WT} samples (supplementary Table S2). A negative normalized enrichment score (NES) indicates signatures enriched more in control cells; a positive NES indicates signatures enriched more in B16^{H350A} cells. The false discovery rate (FDR) is the estimated probability that a signature with a given NES represents a false positive; we considered signatures to be significantly enriched at FDR ≤ 0.05. The GeneRatio is calculated as the fraction of the ranked protein list found in each signature set.

The signaling function of IDO1 is constitutively active in B16^{H350A} melanoma cells

Besides degrading Trp into Kyn, IDO1 triggers non-enzymatic pathways in DCs that can either extend or reduce its own half-life and, consequently, the immunoregulatory effects mediated by itself.[19–21] The phosphorylation of critical tyrosine residues in the ITIMs is required to support this non-enzymatic function. We have previously demonstrated that the enzymatic and the non-enzymatic (namely, signaling) conformations of IDO1 are mutually exclusive since the negative charge exposed by phosphorylated tyrosines in ITIMs distorts the catalytic site and invalidates the activity of the enzyme.[22,31] Therefore, we firstly analyzed whether the null enzyme IDO1^{H350A} was phosphorylated in B16 melanoma cells. To overcome the different protein expressions of IDO1 in B16^{H350A} and B16^{WT} melanoma cell lines, differential amount of WCL was loaded to normalize IDO1 content for immunoprecipitation by means of an antibody specific for the phosphorylated ITIMs of the enzyme.[19,29,32] The results demonstrated that IDO1 is constitutively phosphorylated in B16^{H350A} cells as compared to B16^{WT} samples (Figure 3a). Once phosphorylated in ITIMs, IDO1 acquires the ability to bind different molecular partners, such as SOCS3 and the phosphatases SHP-1 and SHP-2, which are responsible for specific downstream effects.[20] By co-immunoprecipitation experiments, we found in B16 melanoma cells that IDO1^{H350A} was associated with SHP-2 at a significantly higher extent, as compared to IDO1^{WT} (Figure 3b,c), while no differences were observed in the ability to interact with SOCS3 and SHP-1 (data not shown). Since SHP-2 phosphatase promotes Ras activation and the down-stream Erk activation[33,34] in many types of cancer favoring the tumor progression, we analyzed the activation of the Ras/Erk
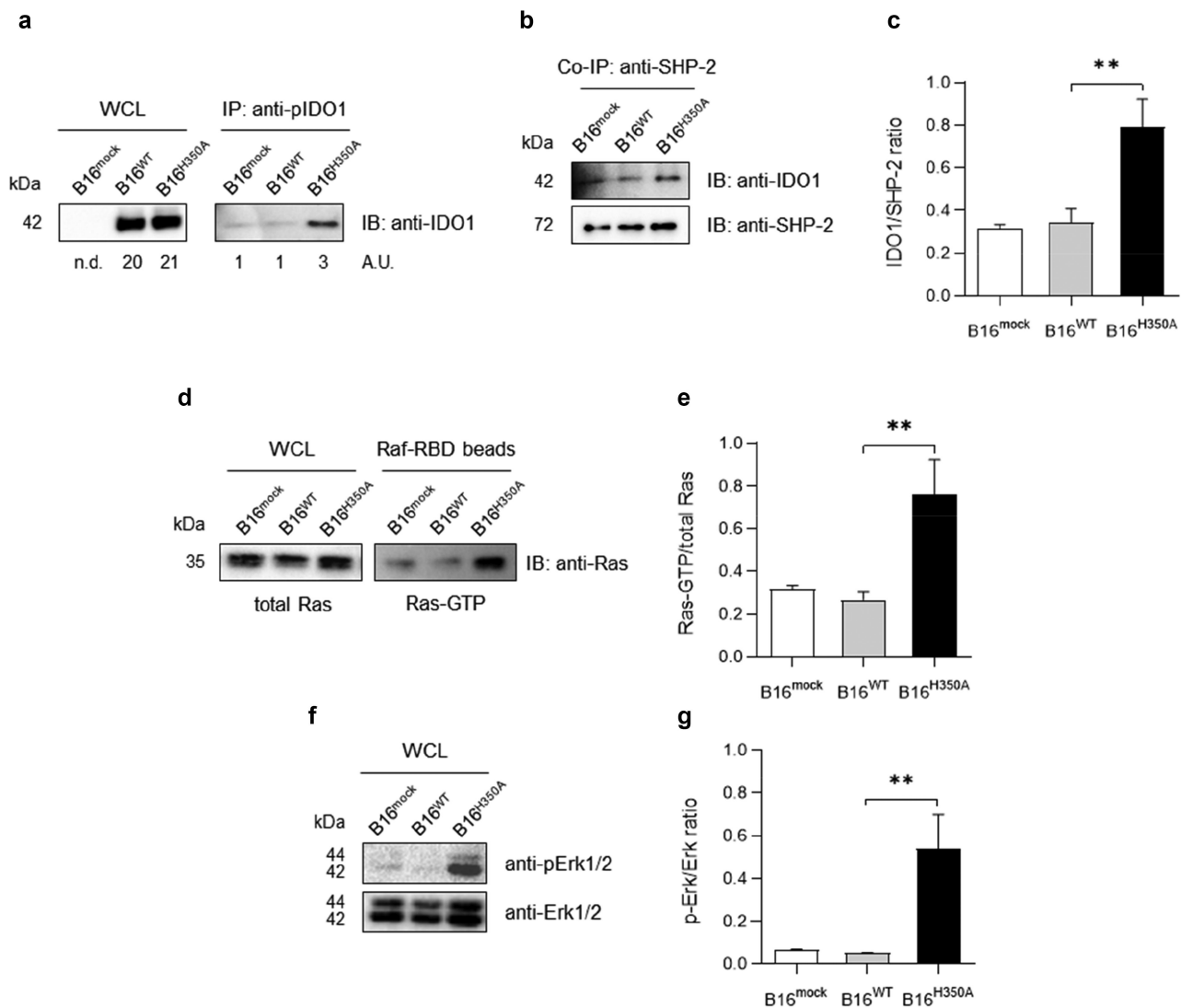

Figure 3. Molecular mediators of the signaling function of the non-enzymatic IDO1 active in B16 ^{H350A} cells. (a-g) Whole cell lysates (WCLs) of stably transfected B16 cell lines (B16^{mock}, B16^{WT}, B16^{H350A}) were normalized for IDO1 content prior to be loaded as WCL, or used for the immunoprecipitation analysis. (a) Immunoblot (IB) with anti-IDO1 and densitometric analysis (A.U., arbitrary units; n.d., not detectable) showing the IDO1 content in WCL (left panel). Immunoprecipitation (IP) of phosphorylated IDO1 with anti-pIDO1 recognizing IDO1 phospho-ITIMs and subsequent immunoblot with anti-IDO1 (right panel). (b-c) Densitometric results of co-immunoprecipitation (Co-IP) with anti-SHP-2 antibody and immunoblot with either anti-IDO1, or anti-SHP-2 (b) are reported as IDO1/SHP-2 ratio (c). (d-e) The relative amount of active Ras (Ras-GTP) over total Ras in stably transfected B16 cell lines is shown by pull-down assay with Raf-RBD beads followed by immunoblot with anti-Ras (d) and reported as Ras-GTP/total Ras ratio (e). Immunoblot with either anti-pErk1/2, or anti-Erk1/2 (f) are reported as ratio of pErk1/2 over Erk1/2 (g). Data (mean ± SD) are the results of three independent measurements. One-way ANOVA was used for the analysis. B16^{H350A} vs B16^{WT}, *P < .05, **P < .01.

pathway within melanoma cells.[35] By pull-down assay and immunoblot analysis, we found that this pathway is constitutively activated in B16[H350A] cells, as shown by the significantly increased expression of active Ras-GTP (Figure 3d,e) and Erk1/2 phosphorylation (Figure 3f,g). At the opposite, the Ras-Erk1/2 axis resulted in switched-off in B16[Y/F] (supplementary Figure S2a, b), a mutant that lost the ITIM-mediated activity of IDO1 protein,[19,21] suggesting that the non-enzymatic activity of IDO1 is required for the constitutive activation of the pathway Ras-Erk1/2 in B16 melanoma.

As a whole, these data suggested that enzyme-null IDO1[H350A] participates and activates the SHP-2/Ras/Erk signaling pathway in B16 melanoma cells.

In vitro growth and malignant progression of B16[H350A] melanoma cells

As the Ras/Erk pathway controls key cellular processes such as proliferation, invasion, and survival that are constitutively activated in human cancers including melanoma,[36,37] we analyzed the *in vitro* behavior of B16[H350A], B16[WT] and B16[mock] cells. We observed a higher proliferative rate in B16[H350A] cells as compared to B16[WT] and B16[mock] counterparts (Figure 4a). Of note, the slower in vitro proliferation of B16[WT] cells, observed in all the original three clones (supplementary Figure S1c), seems independent of the strong depletion of Trp in the cell culture (supplementary Figure S3 A), as the supplementation of exogenous Trp to B16[WT] culture did not affect the proliferation rate (supplementary Figure S3b). The wound healing assay revealed a significantly higher migratory capacity of B16[H350A] cells that reached a 50% and a 100% of wound closure in just over 12 h and 36 h, respectively. By contrast, B16[mock] cells reached the 100% just after 48 h and B16[WT] cells could not close the wound in 48 h (Figure 4b,c). In addition, the soft agar colony formation assay demonstrated a significantly higher capability to grow in an anchorage-independent manner for B16[H350A] cells when compared to B16[WT] and B16[mock] counterparts (Figure 4d,e).

Overall, these data confirmed a faster *in vitro* growth and higher tumorigenic phenotype of B16[H350A] melanoma cells compared to the other B16 melanoma cell lines.

IDO1 enhances tumor growth through the non-enzymatic function

We next characterized the *in vivo* growth of B16[H350A] cells after their subcutaneous implantation into syngeneic mice. Results showed that B16[WT] and B16[mock] tumors have a similar growth rate *in vivo*, while the melanoma tumor growth is significantly accelerated when B16[H350A] cells were implanted (Figure 5a,b). Similar results were also obtained by monitoring the *in vivo* growth of two different clones of B16[H350A], B16[WT], and B16[mock] (supplementary Figure S4). Tumor volumes and weights were both significantly increased in the B16[H350A] compared to B16[WT] and B16[mock]-bearing mice at the time of sacrifice (Figure 5a-d). Moreover, B16[H350A]-bearing mice have a reduced median overall

survival as compared to B16[mock] and B16[WT] tumors (20.5, 27, and >27 days, respectively) (Figure 5e).

To assess whether the observed differences in tumor growth were associated with immune suppression, we measured the number of tumor-infiltrating CD4^{+}, CD8^{+} T lymphocytes producing IFN-γ as well as of regulatory T cells (Tregs). At 2 weeks post-implantation, we found that the absolute number of CD4^{+} cells gated on CD45^{+}CD3^{+} cell population was significantly higher in B16[H350A] than in B16[WT] and B16[mock] tumors, while few CD8^{+} cells were detected in B16[H350A] tumors (Figure 5f). Among the T cells subsets, a significantly lower number of IFN-γ-producing CD4^{+} and CD8^{+} T lymphocytes was counted in B16[H350A] compared to B16[mock] tumors and a significantly higher number of Foxp3^{+} Tregs in B16[H350A] tumors compared to B16[WT] and B16[mock] tumors (Figure 5g). Overall, the immunophenotyping of the xenograft tumors revealed that B16[H350A] were mainly infiltrated by regulatory CD4^{+} Foxp3^{+} T lymphocytes and poorly infiltrated by both IFN-γ-producing CD4^{+} and CD8^{+} T lymphocytes.

On analyzing IDO1 expression and activity in the whole tumor explants, we observed that both B16[WT] and B16[H350A] tumors expressed high levels of the IDO1 protein differently from B16[mock] tumors (Figure 6a,b). Differently from IDO1 expression in the tumor cell lines (Figure 1d), the level of IDO1 protein was significantly higher in B16[WT] than in B16[H350A] explanted tumors, suggesting that the tumor xenografts are infiltrated by cells (other than B16 tumor cells) that can express IDO1 protein. In addition, the high level of Kyn, only detected in B16[WT] homogenate (Figure 6c), could induce the IDO1 expression in the tumor-infiltrating cells. Surprisingly, the *in vivo* growth of B16[H350A] tumor maintained the null enzymatic activity of IDO1 (Figure 6c), excluding the tumor infiltration by the IDO1-competent cells.

We next questioned whether the activation of the SHP-2/Ras/Erk signaling pathway measured *in vitro* might account for the *in vivo* faster growth as well. Results confirmed that B16[H350A] tumors have a constitutive activation of Ras (Figure 6d,e), and a significantly increased phosphorylation of Erk1/2 and expression of SHP-2 (Figure 6f-h).

Overall, these results suggested that the non-enzymatic form of IDO1 is endowed with tumor cell-specific function that relies on the activation of the SHP-2/Ras/Erk signaling pathways fostering the malignant progression of B16[H350A] melanoma.

Discussion

The anti-tumor therapeutic approach inhibiting IDO1 catalytic activity was rationally based on several observations suggesting a crucial involvement of IDO1 in cancer immune escape and progression. Many human tumors express IDO1[38] that is considered a prognostic factor; IDO1-positive mouse tumors were protected from immune rejection;[39] and IDO1 catalytic inhibitors increased the therapeutic efficacy of several pharmacological treatments in multiple preclinical tumor models.[30,40] Although the rational in developing IDO1 catalytic inhibitors is clear, the inadequate response of these compounds – as demonstrated by the recent clinical trials – highlights the urgent need to direct the research on IDO1 biology toward
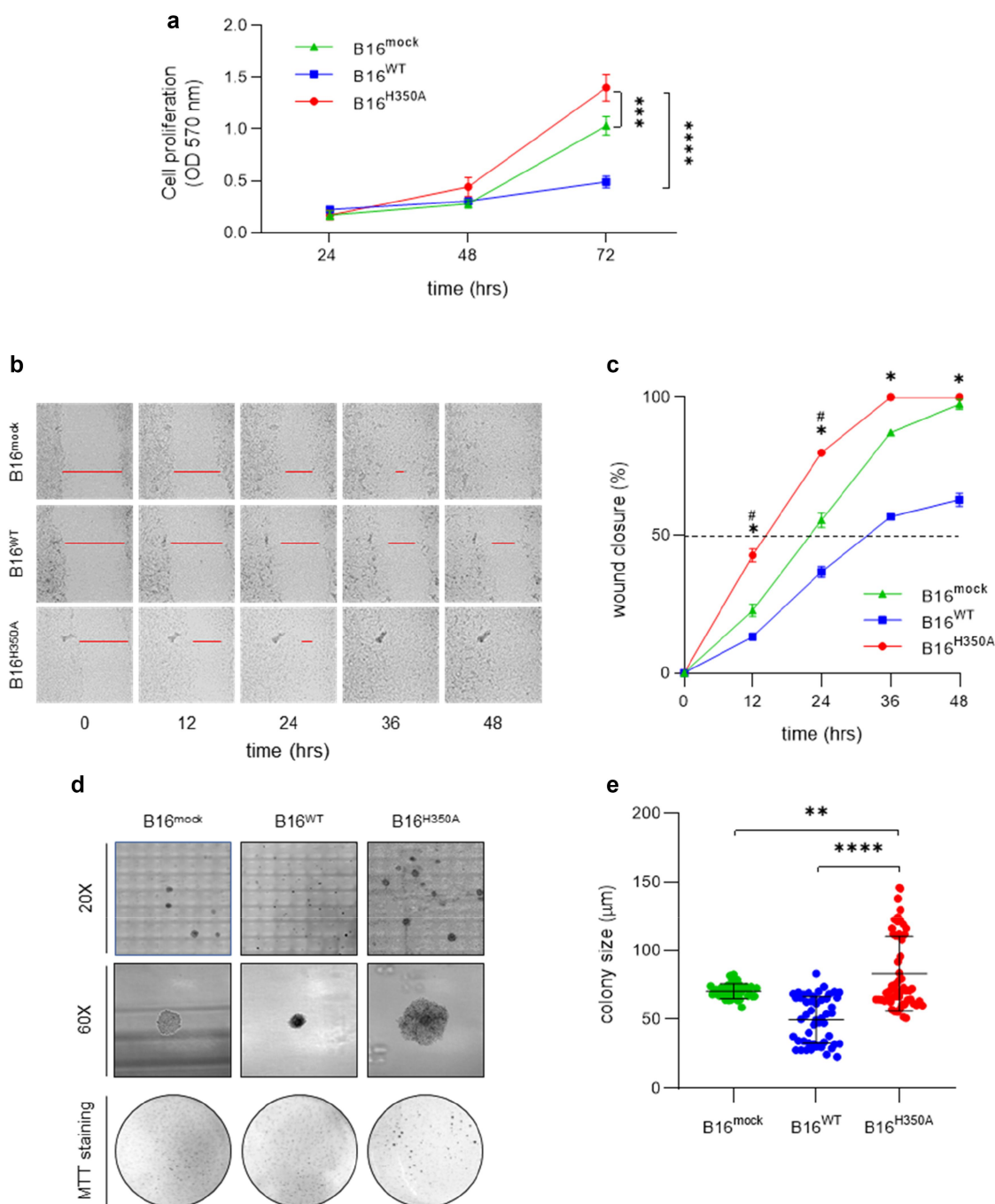
Figure 4. *In vitro* analysis of the tumorigenic phenotype associated with B16H350A cells. (a) *In vitro* cell proliferation of B16mock, B16WT and B16H350A cells incubated in a multiwall plate (5x10^{4} cells/well) and monitored for 24, 48 and 72 hours by MTT assay. (b-c) Time course of scratch closures in B16mock, B16WT and B16H350A cell lines. Cell migration was monitored for 48 hours by scratch test, acquiring the image at 12, 24, 36 and 48 hours (b). The scratch area was expressed as a percentage of the wound closure respect to time zero (c). (d-e) Soft agar colony formation assay in B16mock, B16WT and B16H350A cell lines. Cells were grown in soft agar and, after 14 days, colonies were imaged at low (20X) and high (60X) magnification, and then stained with MTT. Picture are representative of three independent experiments (d). Plotted colony sizes were measured using ImageJ software (e). Data are the means (± S.D.) of two independent experiments each performed in triplicate. Two-way ANOVA (a and c), or one-way ANOVA (**E**) were used for the analysis. B16H350A vs B16WT, *P < .05, **P < .001,***P < .001, ****P < .0001. B16H350A vs B16mock, #P < .05.

a wider field. This emerging awareness has sped up the development of a new generation of efficacious IDO1 inhibitors capable of inhibiting the apo-IDO1 rather than the holo-form.[24,41] The design of the heme-displacing inhibitors of IDO1 is currently a major focus in the field. By this class of inhibitors, investigators firstly provided evidence of a dynamical balance between two different conformations of IDO1, the holo- and the apo-form, similarly to others heme-proteins. Furthermore, Biswas P. et al. have recently demonstrated the biochemical delivery of the intracellular heme to apo-IDO1, describing IDO1 as a heme-protein that can exist naturally, and even predominantly, in its heme-deficient form in the cells.[42]

A growing need for considering the multifaceted functions of both holo- and apo-IDO1 in the tumor microenvironment motivated us to investigate the non-enzymatic activity of
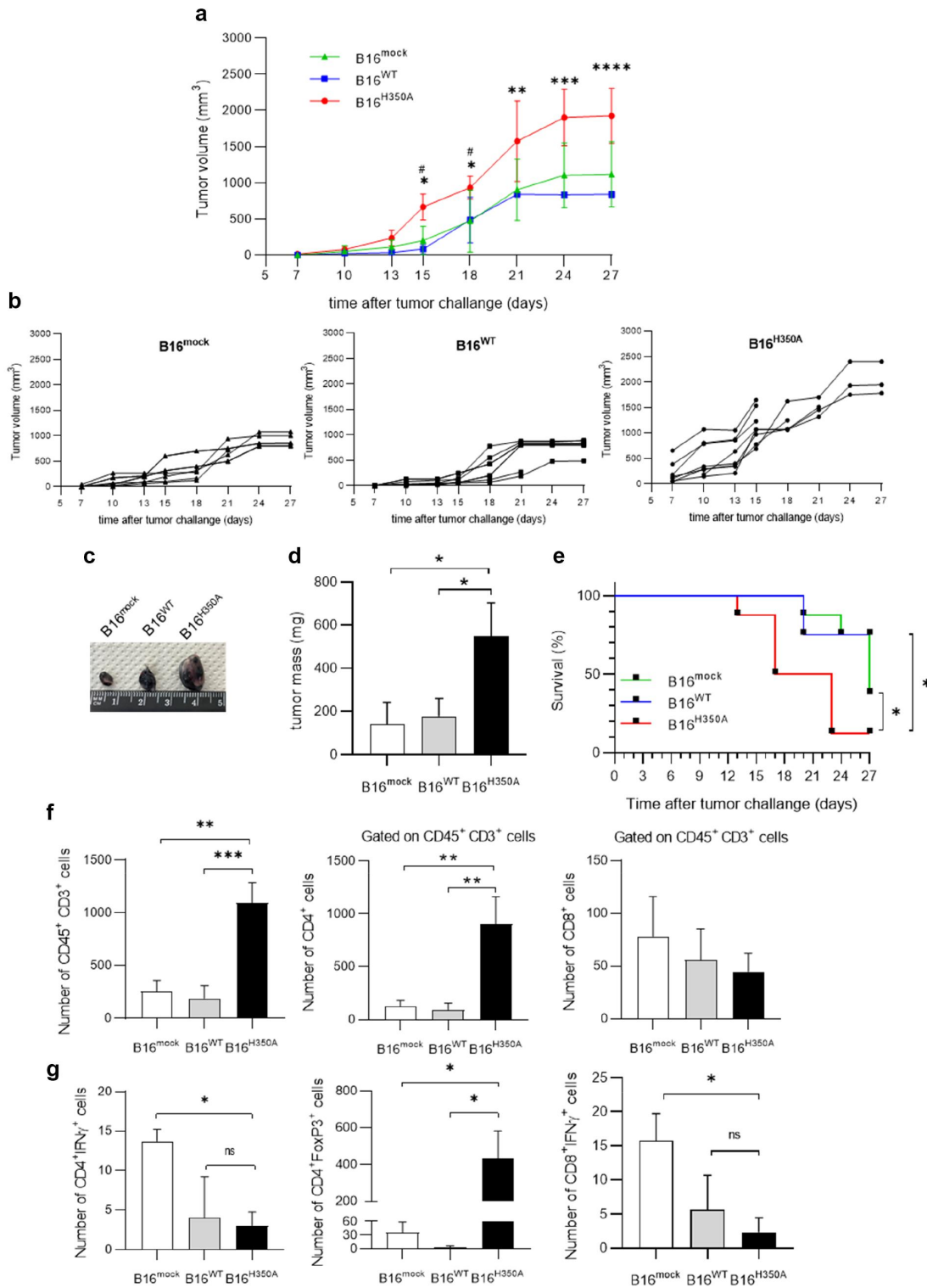
Figure 5. *In vivo* growth and malignant progression of B16^H350A expressing non-enzymatic IDO1. B16^mock, B16^WT or B16^H350A cell suspensions were subcutaneously injected into the flank of C57BL/6 mice. (a) Tumor growth (C57BL/6 mice; n = 8) was monitored 7 days after tumor challenge up to 27 days. Data of tumor volume (mean ± SD) are the result of three independent experiments. (b) B16^mock, B16^WT or B16^H350A tumor volumes of individual mice (n = 8). Representative images (c) and masses (d) of subcutaneous tumors at day 27 are shown. Data of tumor mass (mean ± SD) are the result of three independent experiments. (e) Survival analyses after subcutaneous tumor challenge. Data of overall survival (n = 8, means ± SD) are the result of three independent experiments. (f-g) Flow cytometric analysis of tumor infiltrating lymphocytes. Two weeks after B16^mock, B16^WT or B16^H350A tumor implantation, tumor samples were analyzed. The absolute number of CD45^+CD3^+, CD4^+, CD8^+ cells (f) and of IFNγ^+ CD4^+, IFNγ^+ CD8^+, FoxP3^+ CD4^+ (g) T lymphocytes are shown and quantified (n = 6, means ± SD). Two-way ANOVA (A) and one-way ANOVA (d, f, and g) where used for the analysis. ns, not significant, B16^H350A vs B16^WT, *P < .05, **P < .01 ***P < .001. B16^H350A vs B16^mock, #P < .05. Log-rank test (E) was used to compare survival between B16^H350A, B16^WT and B16^mock groups, *P < .05.
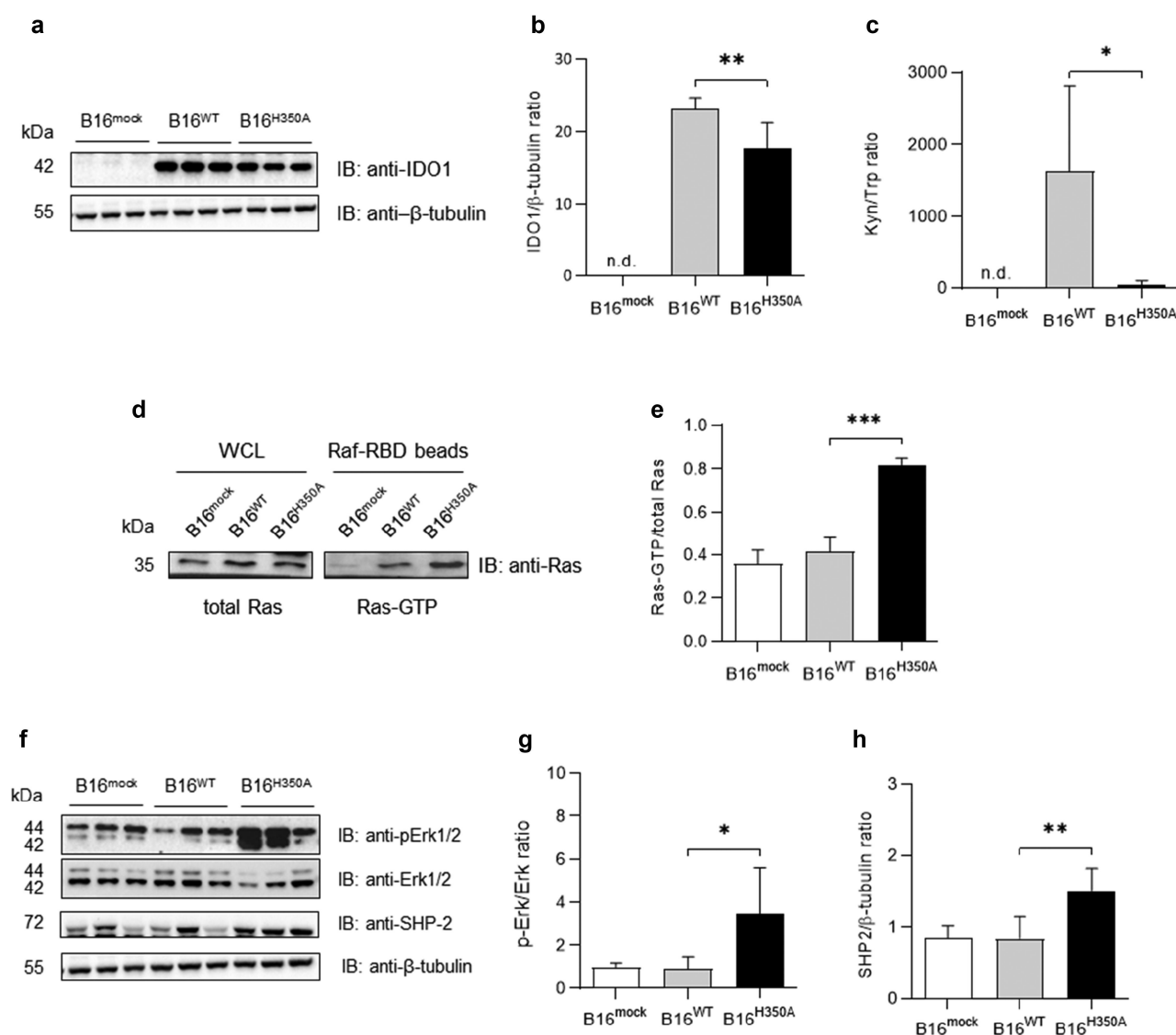
Figure 6. *Ex vivo* analysis of the signaling function of the non-enzymatic IDO1 active in B16^{H350A} tumors. Two weeks after B16^{mock}, B16^{WT} or B16^{H350A} tumor implantation, tumor samples were collected and analyzed. (a) IDO1 protein expression was analyzed in the tumor mass homogenate (n = 3). One representative immunoblot is shown. (b) IDO1/β-tubulin ratio was calculated by densitometric analysis of the specific bands detected in two independent experiments (mean ± S.D.). (c) Kyn and Trp concentration were assessed in tumor homogenate (n = 3) and the Kyn/Trp ratio is represented (means ± S.D.) of two independent experiments. (d) Active Ras (Ras-GTP) was analyzed by pull-down assay in tumor mass homogenate. Total Ras, used for the normalization, and Ras-GTP were detected by anti-Ras western blotting. One representative immunoblot analysis is shown. (e) Ras-GTP/total Ras ratio was calculated by densitometric analysis of the specific bands detected in three independent experiments (mean ± S.D.). (f) SHP-2 and pErk1/2 activation pathway in tumor mass homogenate. Protein expression was analyzed in tumor mass homogenate (n = 3). Total Erk1/2 and β-tubulin were used for pErk1/2 and SHP-2 normalization, respectively. One representative immunoblot analysis is shown. pErk/Erk (g) and SHP-2/β-tubulin (h) ratios were calculated by densitometric analysis of the specific bands detected in two independent experiments (mean ± S.D.). One-way ANOVA followed by post hoc Bonferroni's test was used for the analysis. *P < .05, **P < .01 and ***P < .001.

IDO1^{H350A} mutated protein in the progression of B16 murine melanoma. The amino acid substitution H350A in the murine sequence prevents heme binding and, consequentially, the catalytic function of IDO1. The forced and stable expression of the IDO1^{H350A} protein in B16 melanoma cell line provided a tumor cell model that constitutively expresses the apo-form of IDO1, unable to convert Trp into Kyn and thus with a null catalytic activity. Differently from the physiological turnover of wild-type IDO1 proteins in murine DCs and human PBMCs,[43,44] IDO1^{H350A} has a significantly longer half-life than the wild-type protein within the melanoma cells. The persistence of the null enzyme IDO1 protein in the melanoma cell suggests a functional role of the protein besides its catalytic activity. Moreover, the high level of IDO1^{H350A} protein expression

combined with its longer half-life mirrors an oncogenic behavior. The proteomic analysis confirmed a distinct profile in B16^{H350A} melanoma cells compared to B16^{WT} and B16^{mock}, and the GSEA analysis highlighted statistically significant upregulated gene sets mainly involved in the active cell proliferation and survival, together with down modulated gene sets involved in the activation of the immune response. Therefore, the proteomic analysis unveiled an intrinsic pro-proliferative role of the IDO1^{H350A} protein within the melanoma cells rather than an extrinsic control of the anti-tumor immune response. Although the expression of the catalytically active IDO1 has been often associated with the progression of different tumor types in a microenvironment affected by the metabolic activity of the enzyme,[45,46] the apo-IDO1 protein has never been described as

a switcher of the tumor cell proliferation as an oncogenic signaling. The higher proliferative rate, cell migration capacity, and ability to grow in an anchorage-independent manner of B16[H350A] cells compared to B16[WT] counterpart confirmed this innovative perspective on apo-IDO1 in melanoma cells. Moreover, B16[H350A] cells express a constitutively phosphorylated IDO1 protein capable of better associating SHP-2 phosphatase, identified as one of the molecular partners of IDO1 that mediates its non-enzymatic function in DCs.[19] SHP-2 phosphatase also promotes tumor progression in many types of cancer, including melanoma, because it is a core component of a signaling multi-protein complex that promotes Ras activation and the downstream Erk activation,[33,34] both resulted constitutively activated in B16[H350A] cells compared to B16[WT] tumor. Faster growth and malignant progression of B16[H350A] cells were also detectable *in vivo*, accompanied by a reduction of the anti-tumor immunity. Surprisingly, the *ex vivo* analysis of the explanted tumors revealed that a null catalytic activity was maintained in the B16[H350A] tumor masses after the *in vivo* growth, although the protein expression was still detectable at a high level in the tumor. These observations led us to exclude the infiltration of the tumor by IDO1-competent immune cells or the endogenous induction of a catalytically active form of IDO1 during the *in vivo* progression of B16[H350A] tumor. Moreover, an increased activation of the Ras/Erk pathway was detectable in B16[H350A] tumor homogenates as well as higher levels of the oncogene SHP-2.

Overall, our data describe for the first time a tumor-specific intracellular signaling fostered by IDO1[H350A] in murine melanoma cells and involving the Ras/Erk pathway. The persistence of a phosphorylated form of the apo-IDO1 protein in B16 melanoma promotes its association with SHP-2 phosphatase and the constitutive activation of Ras/Erk signaling, supporting a higher proliferative rate of the tumor.

The unconventional, non-enzymatic activity of IDO1 does not represent a redundant – rather an alternative – mechanism of controlling the immune response.[31,47] The discovery that the IDO1 protein can also act as a transducing molecule, inducing a long-term immunoregulatory phenotype in DCs,[19] combined with the discouraging results from the clinical trials of catalytic IDO1 inhibitors paved new directions in the research activity around this target, in order to make it druggable for the anti-tumor immunity. Bartok et al. elegantly demonstrated that the Trp depletion generated by the IFN-γ-induced catalytic activity of IDO1 promotes in melanoma cells the accumulation of Trp-associated ribosomes that shift the reading frame leading to an aberrant peptide expression on the cell surface.[46] This novel mechanism of IDO1 catalytic activity provides a further layer of complexity to the mechanism of immunosuppression mediated by IDO1. To render even more complex the decryption of the IDO1 role in the tumor microenvironment, we recall its non-enzymatic-mediated immunosuppressive activity in immune cells that can bypass the largely described role of the Trp-Kyn-AhR pathway in cancer development and immunology.[48,49] Recent experimental evidence in the TME described the IDO1 protein in a dynamic balance between its apo- and holo-conformation.[24,26,27] Thus, apo-IDO1 no longer represents

just a transitional conformation for heme cofactor acquisition, but it can become an attractive target.

The data collected in the current manuscript unveil for the first time a tumor-specific non-enzymatic function of IDO1 that contributes to a proliferative signal within the melanoma cell, fostering its tumorigenic phenotype. The pro-tumorigenic IDO1-mediated effect seems to be independent of the catalytic activity, providing a potential explanation to the failure of the catalytic inhibitors of IDO1 in anti-cancer therapy. Probably, the mere catalytic inhibition of IDO1 target in the TME is not sufficient for blocking the tumor development. Our previous data demonstrated that the catalytic and signaling conformations of IDO1 are mutually exclusive.[22,31] This previous observation is in line with the behavior of IDO1[H350A] that mimics a catalytically inactive conformation of the protein and shows constitutive phosphorylation of IDO1 suitable for interacting with transducing molecules. We can thus speculate that the catalytic inhibition of IDO1 could even stabilize the protein in a conformation that, albeit unable to convert Trp into Kyn, is preparatory for the phosphorylation and the activation of an intracellular pathway. Such signaling could induce a tolerogenic phenotype in DCs and a pro-tumorigenic effect in the tumor cells, eventually favoring the tumor cell growth and survival rather than the expected anti-tumor activity. If this is the case, the catalytic inhibition of IDO1 in the TME could even turn worse the anti-tumor response. Besides the catalytic inhibition, novel IDO1-targeted approaches could be developed. Recently, a proteolysis targeting chimera (PROTAC) has been developed and studied in a preclinical model of glioblastoma, showing a therapeutic potential.[50]

It is still unclear if there will be a path forward for the development of efficacious IDO1 catalytic inhibitors in the anti-cancer immunotherapy and certainly, the non-enzymatic activity of this drug target can no longer be neglected in the tumor microenvironment. It is time to change the perspective on IDO1-based drug discovery, by evaluating the effects of the drug candidates on both the catalytic and non-enzymatic functions of this pleiotropic target.

Acknowledgments

Author Contributions

C.O. and G.M. designed the study and interpreted the data; E.O. generated melanoma cell lines and collected the data; E.O., MTP, E.P., S.R. performed the in vitro experiments; C.V. and C.S. performed the in vivo experiments; M.G. performed flow cytometry analysis; S.B. performed the computational analysis of the proteomic data; A.M. performed the statistical analysis; M.L.B. and G.M. drafted the manuscript; C.O. edited and revised the manuscript.

All authors have read and agreed to the published version of the manuscript.

Disclosure statement

Funding

ORCID

C Orabona http://orcid.org/0000-0003-3113-0572

Data availability statement

References

1. Ernst M, Giubellino A. The current state of treatment and future directions in cutaneous malignant melanoma. Biomedicines. 2022 March;10(4):822. doi:10.3390/biomedicines10040822.

2. Olbryt M. Molecular background of skin melanoma development and progression: therapeutic implications. Postepy Dermatol Alergol. 2019;36(2):129–138. doi:10.5114/ada.2019.84590.

3. Kozyra P, Krasowska D, Pitucha M, Barresi V, Di Liberto V, Frinchi M, Bentivoglio M, Condorelli DF. New potential agents for malignant melanoma treatment-most recent studies 2020-2022. Int J Mol Sci. 2022;24(1):23. doi:10.3390/ijms24010023.

4. Siegel RL, Miller KD, Fuchs HE, Jemal A. Cancer Statistics, 2021. CA Cancer J Clin. 2021;71(1):7–33. doi:10.3322/caac.21654.

5. Paluncic J, Kovacevic Z, Jansson PJ, Kalinowski D, Merlot AM, Huang MLH, Lok HC, Sahni S, Lane DJR, Richardson DR, et al. Roads to melanoma: key pathways and emerging players in melanoma progression and oncogenic signaling. Biochim Biophys Acta. 2016;1863(4):770–784. doi:10.1016/j.bbamcr.2016.01.025.

6. Gray-Schopfer V, Wellbrock C, Marais R. Melanoma biology and new targeted therapy. Nature. 2007;445(7130):851–857. doi:10.1038/nature05661.

7. Eddy K, Shah R, Chen S. Decoding melanoma development and progression: identification of therapeutic vulnerabilities. Front Oncol. 2020;10:626129. doi:10.3389/fonc.2020.626129.

8. Ribas A, Wolchok JD. Cancer immunotherapy using checkpoint blockade. Science. 2018;359(6382):1350–1355. doi:10.1126/science.aar4060.

9. Schadendorf D, Hodi FS, Robert C, Weber JS, Margolin K, Hamid O, Patt D, Chen -T-T, Berman DM, Wolchok JD, et al. Pooled analysis of long-term survival data from phase II and phase III trials of ipilimumab in unresectable or metastatic melanoma. J Clin Oncol. 2015;33(17):1889–1894. doi:10.1200/JCO.2014.56.2736.

10. Carretero-González A, Lora D, Ghanem I et al, Analysis of response rate with ANTI PD1/PD-L1 monoclonal antibodies in advanced solid tumors: a meta-analysis of randomized clinical trials. Oncotarget. 2018;9: 8706–8715.

11. Terness P, Bauer TM, Röse L, Dufter C, Watzlik A, Simon H, Opelz G. Inhibition of allogeneic T cell proliferation by indoleamine 2,3-dioxygenase-expressing dendritic cells: mediation of suppression by tryptophan metabolites. J Exp Med. 2002;196 (4):447–457. doi:10.1084/jem.20020052.

12. Munn DH, Mellor AL. Indoleamine 2,3-dioxygenase and tumor-induced tolerance. J Clin Invest. 2007;117(5):1147–1154. doi:10.1172/JCI31178.

13. Mezrich JD, Fechner JH, Zhang X, Johnson BP, Burlingham WJ, Bradfield CA. An interaction between kynurenine and the aryl hydrocarbon receptor can generate regulatory T cells. J Immunol. 2010;185(6):3190–3198. doi:10.4049/jimmunol.0903670.

14. Platten M, Nollen EAA, Röhrig UF, Fallarino F, Opitz CA. Tryptophan metabolism as a common therapeutic target in cancer, neurodegeneration and beyond. Nat Rev Drug Discov. 2019;18 (5):379–401. doi:10.1038/s41573-019-0016-5.

15. Gargaro M, Scalisi G, Manni G, Briseño CG, Bagadia P, Durai V, Theisen DJ, Kim S, Castelli M, Xu CA, et al. Indoleamine 2,3-dioxygenase 1 activation in mature cDC1 promotes tolerogenic education of inflammatory cDC2 via metabolic communication. Immunity. 2022;55(6):1032–1050.e1014. doi:10.1016/j.immuni.2022.05.013.

16. Long GV, Dummer R, Hamid O, Gajewski T, Caglevic C, Dalle S, Arance A, Carlino MS, Grob -J-J, Kim TM, et al. Epacadostat (E) plus pembrolizumab (P) versus pembrolizumab alone in patients (pts) with unresectable or metastatic melanoma: results of the phase 3 ECHO-301/KEYNOTE-252 study. J Clin Oncol. 2018;36 (15_suppl):108. doi:10.1200/JCO.2018.36.15_suppl.108.

17. Eynde B, Baren N, Baurain J-F. Is there a clinical future for IDO1 inhibitors after the failure of epacadostat in melanoma? Ann Rev Cancer Biol. 2020;4(1):241–256. doi:10.1146/annurev-cancerbio-030419-033635.

18. Pallotta MT, Rossini S, Suvieri C, Coletti A, Orabona C, Macchiarulo A, Volpi C, Grohmann U. Indoleamine 2,3-dioxygenase 1 (IDO1): an up-to-date overview of an eclectic immunoregulatory enzyme. Febs J. 2021;289(20):6099–6118. doi:10.1111/febs.16086.

19. Pallotta MT, Orabona C, Volpi C, Vacca C, Belladonna ML, Bianchi R, Servillo G, Brunacci C, Calvitti M, Bicciato S, et al. Indoleamine 2,3-dioxygenase is a signaling protein in long-term tolerance by dendritic cells. Nat Immunol. 2011;12(9):870–878. doi:10.1038/ni.2077.

20. Orabona C, Pallotta MT, Grohmann U. Different partners, opposite outcomes: a new perspective of the immunobiology of indoleamine 2,3-dioxygenase. Mol Med. 2012;18(5):834–842. doi:10.2119/molmed.2012.00029.

21. Orabona C, Pallotta MT, Volpi C, Fallarino F, Vacca C, Bianchi R, Belladonna ML, Fioretti MC, Grohmann U, Puccetti P, et al. SOCS3 drives proteasomal degradation of indoleamine 2,3-dioxygenase (IDO) and antagonizes IDO-dependent tolerogenesis. Proc Natl Acad Sci U S A. 2008;105 (52):20828–20833. doi:10.1073/pnas.0810278105.

22. Albini E, Rosini V, Gargaro M, Mondanelli G, Belladonna ML, Pallotta MT, Volpi C, Fallarino F, Macchiarulo A, Antognelli C, et al. Distinct roles of immunoreceptor tyrosine-based motifs in immunosuppressive indoleamine 2,3-dioxygenase 1. J Cell Mol Med. 2017;21(1):165–176. doi:10.1111/jcmm.12954.

23. Thomas SR, Salahifar H, Mashima R, Hunt NH, Richardson DR, Stocker R. Antioxidants inhibit indoleamine 2,3-dioxygenase in IFN-gamma-activated human macrophages: posttranslational regulation by pyrrolidine dithiocarbamate. J Immunol. 2001;166 (10):6332–6340. doi:10.4049/jimmunol.166.10.6332.

24. Nelp MT, Kates PA, Hunt JT, Newitt JA, Balog A, Maley D, Zhu X, Abell L, Allentoff A, Borzilleri R, et al. Immune-modulating enzyme indoleamine 2,3-dioxygenase is effectively inhibited by targeting its apo-form. Proc Natl Acad Sci U S A. 2018;115 (13):3249–3254. doi:10.1073/pnas.1719190115.

25. Zhai L, Ladomersky E, Dostal CR, Lauing KL, Swoap K, Billingham LK, Gritsina G, Wu M, McCusker RH, Binder DC, et al. Non-tumor cell IDO1 predominantly contributes to enzyme activity and response to CTLA-4/PD-L1 inhibition in mouse glioblastoma. Brain Behav Immun. 2017;62:24–29. doi:10.1016/j.bbi.2017.01.022.

26. Zhai L, Bell A, Ladomersky E, Lauing KL, Bollu L, Nguyen B, Genet M, Kim M, Chen P, Mi X, et al. Tumor cell IDO enhances

immune suppression and decreases survival independent of tryptophan metabolism in glioblastoma. Clin Cancer Res. 2021;27 (23):6514–6528. doi:10.1158/1078-0432.CCR-21-1392.

27. Ladomersky E, Zhai L, Lauing KL, Bell A, Xu J, Kocherginsky M, Zhang B, Wu JD, Podojil JR, Platanias LC, et al. Advanced age increases immunosuppression in the brain and decreases immunotherapeutic efficacy in subjects with glioblastoma. Clin Cancer Res. 2020;26(19):5232–5245. doi:10.1158/1078-0432.CCR-19-3874.

28. Sun L. Advances in the discovery and development of selective heme-displacing IDO1 inhibitors. Expert Opin Drug Discov. 2020;15(10):1223–1232. doi:10.1080/17460441.2020.1781811.

29. Mondanelli G, Bianchi R, Pallotta MT, Orabona C, Albini E, Iacono A, Belladonna ML, Vacca C, Fallarino F, Macchiarulo A, et al. A relay pathway between arginine and tryptophan metabolism confers immunosuppressive properties on dendritic cells. Immunity. 2017;46(2):233–244. doi:10.1016/j.immuni.2017.01.005.

30. Holmgaard RB, Zamarin D, Munn DH, Wolchok JD, Allison JP. Indoleamine 2,3-dioxygenase is a critical resistance mechanism in antitumor T cell immunotherapy targeting CTLA-4. J Exp Med. 2013;210(7):1389–1402. doi:10.1084/jem.20130066.

31. Albini E, Coletti A, Greco F, Pallotta MT, Mondanelli G, Gargaro M, Belladonna ML, Volpi C, Bianchi R, Grohmann U, et al. Identification of a 2-propanol analogue modulating the non-enzymatic function of indoleamine 2,3-dioxygenase 1. Biochem Pharmacol. 2018;158:286–297. doi:10.1016/j.bcp.2018.10.033.

32. Volpi C, Mondanelli G, Pallotta MT, Vacca C, Iacono A, Gargaro M, Albini E, Bianchi R, Belladonna ML, Celanire S, et al. Allosteric modulation of metabotropic glutamate receptor 4 activates IDO1-dependent, immunoregulatory signaling in dendritic cells. Neuropharmacology. 2016;102:59–71. doi:10.1016/j.neuropharm.2015.10.036.

33. Zhang J, Zhang F, Niu R. Functions of Shp2 in cancer. J Cell Mol Med. 2015;19(9):2075–2083. doi:10.1111/jcmm.12618.

34. Grossmann KS, Rosário M, Birchmeier C, Birchmeier W. The tyrosine phosphatase Shp2 in development and cancer. Adv Cancer Res. 2010;106:53–89.

35. Zhang RY, Yu ZH, Zeng L, Zhang S, Bai Y, Miao J, Chen L, Xie J, Zhang Z-Y. SHP2 phosphatase as a novel therapeutic target for melanoma treatment. Oncotarget. 2016;7(45):73817–73829. doi:10.18632/oncotarget.12074.

36. Santarpia L, Lippman SM, El-Naggar AK. Targeting the MAPK-RAS-RAF signaling pathway in cancer therapy. Expert Opin Ther Targets. 2012;16(1):103–119. doi:10.1517/14728222.2011.645805.

37. Nazarian R, Shi H, Wang Q, Kong X, Koya RC, Lee H, Chen Z, Lee M-K, Attar N, Sazegar H, et al. Melanomas acquire resistance to B-RAF(V600E) inhibition by RTK or N-RAS upregulation. Nature. 2010;468(7326):973–977. doi:10.1038/nature09626.

38. Théate I, van Baren N, Pilotte L, Moulin P, Larrieu P, Renauld J-C, Hervé C, Gutierrez-Roelens I, Marbaix E, Sempoux C, et al. Extensive profiling of the expression of the indoleamine 2,3-dioxygenase 1 protein in normal and tumoral human tissues. Cancer Immunol Res. 2015;3(2):161–172. doi:10.1158/2326-6066.CIR-14-0137.

39. Uyttenhove C, Pilotte L, Théate I, Stroobant V, Colau D, Parmentier N, Boon T, Van den Eynde BJ. Evidence for a tumoral immune resistance mechanism based on tryptophan degradation by indoleamine 2,3-dioxygenase. Nat Med. 2003;9 (10):1269–1274. doi:10.1038/nm934.

40. Feng X, Liao D, Liu D, Ping A, Li Z, Bian J. Development of Indoleamine 2,3-Dioxygenase 1 inhibitors for cancer therapy and beyond: a recent perspective. J Med Chem. 2020;63 (24):15115–15139. doi:10.1021/acs.jmedchem.0c00925.

41. Liu W, Zou Y, Li K, Zhong H, Yu L, Ge S, Lai Y, Dong X, Xu Q, Guo W, et al. Apo-form selective inhibition of IDO for tumor immunotherapy. J Immunol. 2022;209(1):180–191. doi:10.4049/jimmunol.2100938.

42. Biswas P, Dai Y, Stuehr DJ. Indoleamine dioxygenase and tryptophan dioxygenase activities are regulated through GAPDH- and Hsp90-dependent control of their heme levels. Free Radic Biol Med. 2022;180:179–190. doi:10.1016/j.freeradbiomed.2022.01.008.

43. Mondanelli G, Albini E, Pallotta MT, Volpi C, Chatenoud L, Kuhn C, Fallarino F, Matino D, Belladonna ML, Bianchi R, et al. The proteasome inhibitor bortezomib controls indoleamine 2,3-Dioxygenase 1 breakdown and restores immune regulation in autoimmune diabetes. Front Immunol. 2017;8:428. doi:10.3389/fimmu.2017.00428.

44. Mondanelli G, Di Battista V, Pellanera F, Mammoli A, Macchiarulo A, Gargaro M, Mavridou E, Matteucci C, Ruggeri L, Orabona C, et al. A novel mutation of indoleamine 2,3-dioxygenase 1 causes a rapid proteasomal degradation and compromises protein function. J Autoimmun. 2020;115:102509. doi:10.1016/j.jaut.2020.102509.

45. Holmgaard RB, Zamarin D, Li Y, Gasmi B, Munn D, Allison J, Merghoub T, Wolchok J. Tumor-expressed IDO recruits and activates MDSCs in a treg-dependent manner. Cell Rep. 2015;13 (2):412–424. doi:10.1016/j.celrep.2015.08.077.

46. Bartok O, Pataskar A, Nagel R, Laos M, Goldfarb E, Hayoun D, Levy R, Körner P-R, Kreuger IZM, Champagne J, et al. Anti-tumour immunity induces aberrant peptide presentation in melanoma. Nature. 2021;590(7845):332–337. doi:10.1038/s41586-020-03054-1.

47. Zhai L, Bell A, Ladomersky E, Lauing KL, Bollu L, Sosman JA, Zhang B, Wu JD, Miller SD, Meeks JJ, et al. Immunosuppressive IDO in cancer: mechanisms of action, animal models, and targeting strategies. Front Immunol. 2020;11:1185. doi:10.3389/fimmu.2020.01185.

48. Campesato LF, Budhu S, Tchaicha J, Weng C-H, Gigoux M, Cohen IJ, Redmond D, Mangarin L, Pourpe S, Liu C, et al. Blockade of the AHR restricts a Treg-macrophage suppressive axis induced by L-Kynurenine. Nat Commun. 2020;11(1):4011. doi:10.1038/s41467-020-17750-z.

49. Atene CG, Fiorcari S, Mesini N, Alboni S, Martinelli S, Maccaferri M, Leonardi G, Potenza L, Luppi M, Maffei R, et al. Indoleamine 2, 3-Dioxygenase 1 mediates survival signals in chronic lymphocytic leukemia via kynurenine/aryl hydrocarbon receptor-mediated MCL1 modulation. Front Immunol. 2022;13:832263. doi:10.3389/fimmu.2022.832263.

50. Bollu LR, Bommi PV, Monsen PJ, Zhai L, Lauing KL, Bell A, Kim M, Ladomersky E, Yang X, Platanias LC, et al. Identification and characterization of a novel indoleamine 2,3-Dioxygenase 1 protein degrader for glioblastoma. J Med Chem. 2022;65 (23):15642–15662. doi:10.1021/acs.jmedchem.2c00771.